

AperTO - Archivio Istituzionale Open Access dell'Università di Torino

Superoxide-driven autocatalytic dark production of hydroxyl radicals in the presence of complexes of natural dissolved organic matter and iron

This is the author's manuscript

Original Citation:

Availability:

This version is available <http://hdl.handle.net/2318/1932291> since 2024-11-25T09:05:17Z

Published version:

DOI:10.1016/j.watres.2020.115782

Terms of use:

Open Access

Anyone can freely access the full text of works made available as "Open Access". Works made available under a Creative Commons license can be used according to the terms and conditions of said license. Use of all other works requires consent of the right holder (author or publisher) if not exempted from copyright protection by the applicable law.

(Article begins on next page)

1 Superoxide-driven autocatalytic dark production of
2 hydroxyl radicals in the presence of complexes of
3 natural dissolved organic matter and iron

4 *Yihua Xiao*^{1*}, *Luca Carena*², *Marja-Terttu Näsi*¹, *Anssi V. Vähätalo*¹

5 ¹Department of Biological and Environmental Science, University of Jyväskylä, 40014
6 Jyväskylä, Finland

7 ²Dipartimento di Chimica, Università di Torino, Via Pietro Giuria 5, 10125 Torino, Italy

8

9 *Corresponding author: yihua.y.xiao@jyu.fi

10

11

Abstract

We introduced superoxide as potassium superoxide (KO_2) to artificial lake water containing dissolved organic matter (DOM) without or with introduced ferric iron complexes (DOM-Fe), and monitored the production rate of hydroxyl radicals as well as changes in the absorption and fluorescence properties of DOM. The introduction of KO_2 decreased the absorption by DOM but increased the spectral slope coefficient of DOM more with complexed ferric Fe than without it. The introduction of KO_2 increased the fluorescence of humic-like components in DOM without introduced ferric Fe but resulted in the loss of fluorescence in DOM with introduced ferric Fe. A single introduction of $13 \mu\text{mol L}^{-1}$ KO_2 produced $10 \mu\text{mol L}^{-1}$ and $104 \mu\text{mol L}^{-1}$ hydroxyl radicals during a week-long experiment without and with the introduced DOM-Fe complexes, respectively. The production rate of hydroxyl radicals decreased exponentially with time but levelled off and continued several days in DOM with introduced ferric Fe. These findings suggest that in the presence of DOM-Fe complexes, superoxide can trigger an autocatalytic Fenton reaction that produces hydroxyl radicals and breaks down DOM.

Keywords: dissolved organic matter, iron, superoxide, hydroxyl radicals, production rate, absorption

1 Introduction

Dissolved organic matter (DOM) is a heterogeneous mixture of organic compounds and plays important roles in natural and engineered systems. In soils and freshwaters, the majority of DOM consists of humic substances that primarily originate from terrestrial plant litter after biotic and abiotic transformations (Piccolo, 1996; Tranvik, 1988). Humic DOM binds ferric iron, Fe(III), into complexes, DOM-Fe(III), and keeps poorly soluble Fe(III) in dissolved form (Fujii et al., 2014). Humic DOM contains aromatic and quinone-like moieties, which occur in three redox-states (quinones, semiquinones and hydroquinones) and can mediate reactions between electron donors and acceptors with Fe (Aeschbacher et al., 2010; Chen & Pignatello, 1997; Garg et al., 2018; Yuan et al., 2016).

The enzymatic hydrolysis of humic DOM and its intracellular metabolism is inefficient, because the large size of molecular aggregates, chemical heterogeneity, and non-hydrolysable bonds limit the microbial transformation of humic DOM (Arnosti, 2004). Abiotic photochemical reactions mineralize humic DOM and account for one tenth of CO₂ emissions in freshwaters (Aarnos et al., 2018; Koehler et al., 2014). The remaining 90% of DOM is mineralized through mechanisms that are poorly known.

Extracellular reactions between DOM and reactive oxygen species (ROS) can explain a part of DOM transformations (Mostovaya et al., 2017; Page et al., 2012; Trusiak et al., 2018; Waggoner et al., 2017). The first step in the formation of ROS is a one-electron reduction of O₂ to superoxide (O₂^{•-}). Numerous processes produce O₂^{•-}: (i) photochemical reactions (Micinski et al., 1993; Fujii & Otani, 2017; Zhang & Blough, 2016; Text SIV in supporting information (SI)), (ii) abiotic dark oxidation of reduced metals or organic matter (Garg et al., 2018; Gil-Lozano et al., 2017; Page et al., 2012; Yuan et al., 2016) and (iii) biological processes both in light and dark (Diaz et al., 2013; Diaz & Plummer, 2018; Imlay, 2004; Zhang et al., 2016). O₂^{•-} reacts with the redox-active metals (e.g., Fe and copper) and quinone-like moieties

of DOM, but it has otherwise limited reactivity with aqueous DOM (Garg et al., 2011, 2018; Hayyan et al., 2016; Yuan et al., 2016).

$O_2^{\bullet-}$ can be reduced further to hydrogen peroxide (H_2O_2) and hydroxyl radicals ($\bullet OH$). Bimolecular disproportionation and the disproportionation catalyzed by reduced metals or DOM transform $O_2^{\bullet-}$ to H_2O_2 (Goldstone & Voelker, 2000; Ma et al., 2010). $O_2^{\bullet-}$ can reduce DOM-Fe(III) to DOM-Fe(II) (Rose & Waite, 2005). DOM-Fe(II) as well as inorganic Fe(II) can react with H_2O_2 through the Fenton reaction and produce highly reactive $\bullet OH$ that breaks down DOM (Southworth & Voelker, 2003; Voelker et al., 1997).



According to the stoichiometry of the Fenton reaction (Eq. 1), the Fe(III)-catalyzed production of $\bullet OH$ requires three $O_2^{\bullet-}$ radicals, two for the formation of H_2O_2 and one for the formation of DOM-Fe(II). However, the stoichiometry of the Fenton reaction ($\bullet OH$ -to- $O_2^{\bullet-}$ ratio = 0.33) ignores a well-known fact that $\bullet OH$ generates radical species that can regenerate the Fenton reactants and autocatalyze the Fenton reaction (e.g., Chen & Pignatello, 1997; Gil-Lozano et al., 2017). The degree of autocatalysis is poorly known, although it has high importance when the efficiency of the Fenton reaction is evaluated in natural or engineered systems.

The present study estimates the dark production rates of $\bullet OH$ in artificial lake water from $O_2^{\bullet-}$ (introduced as potassium superoxide, KO_2) in the presence of DOM with or without introduced Fe(III). The production rates of $\bullet OH$ were quantified from the reaction between $\bullet OH$ and coumarin (Louit et al., 2005) and after accounting for the major scavengers of $\bullet OH$ in the artificial lake water. In this study we demonstrate that the cumulative production of $\bullet OH$ from $O_2^{\bullet-}$ in a-week-long experiment exceeds the $\bullet OH$ yield of the Fenton reaction by several folds and extensively modifies the spectroscopic properties of DOM.

2 Materials and methods

2.1 Materials and reagents

DOM was extracted from a water sample collected during the fall turnover of Lake Valkea-Kotinen in southern Finland. This small headwater lake is acidic (pH 5.4) with high concentration of DOC ($10\text{--}12\text{ mg DOC L}^{-1} = \sim 20\text{ mg DOM L}^{-1}$) and total Fe ($\sim 5\text{ }\mu\text{M}$; Einola et al., 2011; Vähätalo et al., 2003). In Lake Valkea-Kotinen, the mean molecular mass of DOM is $1130\text{--}4000\text{ g mol}^{-1}$, the content of humic substances and aromatic groups is 75% and 45–67%, respectively (Vogt et al., 2004).

The extraction of DOM followed the method by Dittmar et al. (2008) but included an addition of 0.01 M sodium fluoride (NaF, Sigma-Aldrich) in filtered ($<0.2\text{ }\mu\text{m}$) and acidified (pH 2) lake water. At pH 2, Fe(III) binds poorly on DOM and preferentially forms ferric fluoride complex (Gao & Zepp, 1998). Ferric fluoride and fluoride ions were rinsed out of the column with 0.01 M HCl (Dittmar et al. 2008) to yield extracted DOM with a very low content of fluoride and Fe. The extraction removed 96.6% of Fe from lake water and the DOM extracts contained 8.5 nmol Fe/mg DOM (Table 1). The chemicals ($>97\%$ pure) were bought from Sigma Aldrich. Iron(III) chloride hexahydrate ($\text{FeCl}_3 \cdot 6\text{H}_2\text{O}$) and KO_2 were the sources of Fe(III) and $\text{O}_2^{\bullet-}$, respectively. Coumarin and 7OH-coumarin were the probes for $\bullet\text{OH}$ (Burgos Castillo et al., 2018). The aqueous solutions were prepared in ultrapure water (resistivity $18\text{ M}\Omega\cdot\text{cm}$; SG ultrapure water system, SG WATER), but were later modified to artificial lake water by a salt solution mixture (Table S1). Glassware was soaked overnight in 0.1 M HCl and carefully rinsed with ultrapure water six times prior to use.

2.2 Experimental setup

The experiment consisted of four treatments prepared in triplicates (Table 1):

- 1) “control” – extracted DOM (8.5 nmol Fe/mg DOM) dissolved in artificial lake water;
- 2) “ KO_2 ” – like (1) but with introduced KO_2 ;

3) “Fe” – like (1) but Fe(III) was introduced as DOM-Fe(III) (1000 nmol Fe(III)/mg DOM);

4) “Fe + KO₂” – a combination of (2) and (3).

For the preparation of DOM-Fe(III), the acidic (pH 2) DOM solution (50 mg L⁻¹ in ultrapure water) received 1 mM Fe(III) and was titrated to pH 5 with NaOH and HCl, approximating the ambient pH of Lake Valkea-Kotinen. During the titration, the binding sites of DOM suppressed the hydrolysis of ferric Fe and DOM-Fe(III) was formed (Karlsson & Persson, 2012). According to an equilibrium speciation model (Visual Minteq 3.1), the DOM extract was able to bind Fe(III) entirely and accordingly visual precipitates were absent at any phase of the experiment. The “control” and “KO₂” treatments were titrated in the same way but without the introduced Fe. All treatments received the stock solution of coumarin to the final concentration of 10 µM (Table 1) and inorganic component of artificial lake water (Table S1).

The “KO₂” and “Fe + KO₂” treatments received an alkaline solution of KO₂ (2 g KO₂ in 100 mL 0.05 M NaOH) to a 13 µM final concentration (Table 1). Similar magnitudes of O₂^{•-} form instantly during the oxidation of reduced organic matter or metals (Liao et al., 2019; Minella et al., 2015; Page et al., 2013; Trusiak et al., 2018; Zhang & Yuan, 2017), with a few days of microbial metabolism (Zhang et al., 2016) or with 0.17–few days of solar irradiation depending on water quality (Cooper & Zika, 1983; Micinski et al., 1993; Text SIV in SI). The introduction of KO₂ increased the pH of non-buffered artificial lake water to 12.2, where the reduction rate of DOM-Fe(III) to DOM-Fe(II) by O₂^{•-} is faster than bimolecular disproportionation of O₂^{•-} (see Text SI in SI). The reaction medium was titrated back to pH 5 with HCl. Finally, all treatments were incubated at 20 °C in the dark with a headspace of air.

2.3 UV-Vis spectral analysis

After 26 h and a week (168 h) of incubation, the absorbance of chromophoric DOM

(CDOM) was measured with a UV-Vis spectrometer (Lambda 850, PerkinElmer) from 200 nm to 700 nm at 1 nm intervals. The absorption coefficient was calculated as,

$$a_{\lambda} = 2.303 \times A_{\lambda}/L \quad \text{Eq. 2,}$$

where a_{λ} (m^{-1}) is the absorption coefficient at wavelength λ , A_{λ} (unitless) is absorbance, and L is the path length of the cuvette ($L = 0.01$ m). The changes in a_{λ} were quantified at 410 nm as a_{410} , an indicator of water color (Hongve et al., 2004). The spectral slope coefficient ($S_{275-295}$), which indicates the molecular mass of DOM, was calculated from ln-transformed absorption coefficient between 275 nm and 295 nm (Helms et al., 2008).

2.4 Fluorescence analysis and PARAFAC

Samples for fluorescence analysis were stored at 4 °C after collection and measured within 3 weeks. Fluorescence EEMs were measured with a LS 55 luminescence spectrometer (PerkinElmer). The samples were scanned with an excitation wavelength (Ex) from 240 nm to 450 nm at 5 nm intervals and emission wavelength (Em) from 300 nm to 600 nm with 0.5 nm intervals. The slit width for both Ex and Em was set to 5 nm. Blank and Raman samples from ultrapure water were measured prior to actual samples (Murphy et al., 2003).

PARAllel FACtor analysis (PARAFAC) was run in Matlab R2015b (Mathworks, USA) using the drEEM toolbox (version 0.3.0). The raw EEM dataset ($n = 48$) was corrected for spectral bias, inner filter effects and background signals (measured with ultrapure water). In the end, all EEMs were normalized to the area of Raman peak collected with ultrapure water at Ex = 275 nm to compensate for daily fluctuations in lamp intensity (Kothawala et al., 2016; Murphy et al., 2013). The fluorescent components were validated with multiple split-half tests. The validation was constrained by a Tucker congruence coefficient (TCC >0.95). Finally, the maximum fluorescence intensities (F_{max} , in Raman unit, R.U.) of components were reported.

2.5 Calculations of the cumulative production of •OH radicals

The samples for the quantification of coumarin and 7OH-coumarin were collected at 0,

3, 6, 20, 26, and 168 h. These samples were frozen immediately after collection and analyzed later. Coumarin and 7OH-coumarin were measured by high performance liquid chromatography (HPLC) equipped with UV-Vis absorbance and fluorescence detectors (Louit et al., 2005). The quantification of the two compounds was carried out by means of the UV-Vis absorbance detector for coumarin (absorption wavelength = 280 nm) and fluorescence detector for 7OH-coumarin (excitation wavelength = 320 nm; emission wavelength = 450 nm). The Text SII in SI reports the details of HPLC technique.

The formation rates of $\bullet\text{OH}$ were quantified from the reaction between coumarin and $\bullet\text{OH}$. This reaction has a second-order rate constant of $5.6 \times 10^9 \text{ M}^{-1} \text{ s}^{-1}$ and produces a few hydroxycoumarin isomers, including 7OH-coumarin with a yield of 0.047 (Burgos Castillo et al., 2018). We calculated the production rates of $\bullet\text{OH}$ along the course of the experiment by quantifying periodically the concentrations of 7OH-coumarin and coumarin as well as accounting for the scavenging of $\bullet\text{OH}$ by DOM, Cl^- , HCO_3^- , coumarin and 7OH-coumarin. The calculations assumed a steady-state between the scavenging and the formation rate of $\bullet\text{OH}$. The production rates of $\bullet\text{OH}$ radicals were integrated over the course of the experiment for the cumulative production of $\bullet\text{OH}$. The detailed procedure for calculations is described in the SI.

2.6 Statistical analyses

The statistical difference between the triplicated treatments and control (DOM alone treatment) was assessed using paired t tests with two-tailed distributions. The significance level was set at $P < 0.05$.

3 Results

3.1 Changes in absorption spectra

The introduction of KO_2 did not change the absorption coefficient a_{410} in an early phase of the experiment (at 26 h) but decreased it by 25% by the end of the experiment (at 168 h) compared to DOM in artificial lake water without KO_2 (“control” vs “ KO_2 ”, Figure 1a). In the

“Fe” treatment, the introduced DOM-Fe(III) consistently kept a_{410} at a higher level than in the control (Figure 1a). When introduced with DOM-Fe(III), KO_2 decreased a_{410} by 18% already at 26 h and by 66% over the entire experiment compared to the control (“Fe + KO_2 ”, Figure 1a).

In comparison with the control treatment, KO_2 increased the spectral slope coefficient ($S_{275-295}$), while DOM-Fe(III) decreased it (Figure 1b). When introduced with Fe, KO_2 increased $S_{275-295}$ by 20% at 26 h and by 54% at the end of the experiment (Figure 1b).

3.2 Changes in fluorescent intensities of PARAFAC components

The four components of fluorescent DOM identified by the EEM-PARAFAC associated with humic substances (Comp 1–2, Figure 2 and Table S2), 7OH-coumarin (Comp 3; Figure S1) and protein-like DOM (Comp 4, Figure 2 and Table S2). After 168 h, the introduction of KO_2 had increased the fluorescence of humic-like components 1 and 2 by 39% and 18%, respectively, in comparison to the control treatment (“ KO_2 ”, Figure 3). The added associated Fe(III) quenched the fluorescence of humic-like components 1–2 (“Fe”, Figure 3). In the presence of DOM-Fe(III), KO_2 reduced the fluorescence of components 1–2 relative to the control treatment and decreased the fluorescence of component 4 to negligible level (“Fe + KO_2 ”, Figure 3). Component 3 was detected in all treatments (Figure 3) indicating that $\bullet OH$ radicals transformed coumarin (Table 1) into 7OH-coumarin, as explained in the following section.

3.3 Production of $\bullet OH$

The formation rate of $\bullet OH$, $R_f^{\bullet OH}(t)$, was assessed from the measured concentrations of coumarin and 7OH-coumarin (Figure SIII-1&2) accounting for the other scavengers of $\bullet OH$ as described in the Text SIII in SI. In the beginning of the experiment, $R_f^{\bullet OH}(t_0)$ was 0.0031–0.0034 nM s⁻¹ in the “Fe” treatment and the control, which did not receive KO_2 (Figure

4; Table SIII-1). The introduction of KO_2 resulted in $R_f^{\bullet\text{OH}}(t_0)$ of 0.039 nM s^{-1} and 1.14 nM s^{-1} in the “ KO_2 ” and “ $\text{KO}_2 + \text{Fe}$ ”-treatments, respectively (Figure 4; Table SIII-1). In the “ $\text{KO}_2 + \text{Fe}$ ” treatment, the measured $R_f^{\bullet\text{OH}}(t_0)$ was nearly identical to the corresponding rate of 1.05 nM s^{-1} calculated based on a simple kinetic model (Figure SI-2). Briefly, the calculated rates are based on the kinetics for the following sequence of reactions: (i) the reduction of DOM-Fe(III) to $13 \text{ }\mu\text{M}$ DOM-Fe(II) by $\text{O}_2^{\bullet-}$, (ii) the reduction of O_2 to $\text{O}_2^{\bullet-}$ by DOM-Fe(II), (iii) the disproportionation of $\text{O}_2^{\bullet-}$ to H_2O_2 and (iv) the Fenton reaction (Eq. 1) between H_2O_2 and DOM-Fe(II). The good match between the measured and the calculated $R_f^{\bullet\text{OH}}(t_0)$ in the “ $\text{KO}_2 + \text{Fe}$ ” treatment suggest that, (i) $\text{O}_2^{\bullet-}$ induced the formation of $\bullet\text{OH}$ in the presence of DOM-Fe(III) and (ii) the reaction stoichiometry (e.g., $\bullet\text{OH}$ -to- $\text{O}_2^{\bullet-}$ ratio = 0.33 of Eq. 1) described the measured initial rates well.

The formation rates of $\bullet\text{OH}$ decreased exponentially with time in all treatments, and after 10 h levelled at 0.15 nM s^{-1} in the “ $\text{KO}_2 + \text{Fe}$ ” treatment (Figure 4, Table SIII-1). In the “ $\text{KO}_2 + \text{Fe}$ ” treatment, the prolonged formation of $\bullet\text{OH}$ is consistent with the changes in DOM that took place mostly after 26 h (Figure 1), but inconsistent with a simple kinetic model (Text SI-3). The simple kinetic model incorrectly suggests the depletion of $R_f^{\bullet\text{OH}}(t)$ within a few minutes (Text SI-3) in contrast to the measured $R_f^{\bullet\text{OH}}(t)$, which lasted tens of hours (Figure 4).

The cumulative production of $\bullet\text{OH}$ was computed as the integral of $R_f^{\bullet\text{OH}}(t)$ for the first 10 hours or for the entire length of the experiment (168 h, Table 2, Eq. SIII-1). In all treatments, the majority of $\bullet\text{OH}$ was produced after 10 h (Table 2). In the treatments with introduced KO_2 , the cumulative production of $\bullet\text{OH}$ was 9.9 and $104 \text{ }\mu\text{M}$ in the “ KO_2 ” and “ $\text{KO}_2 + \text{Fe}$ ” treatments, respectively, over the entire length of the experiment (Table 2). The yields of $\bullet\text{OH}$ per introduced $13 \text{ }\mu\text{M}$ KO_2 were $0.76 \bullet\text{OH}/\text{O}_2^{\bullet-}$ and $8 \bullet\text{OH}/\text{O}_2^{\bullet-}$ in the “ KO_2 ” and “ $\text{KO}_2 + \text{Fe}$ ” treatments, respectively. The measured yields exceeded the stoichiometric yield (0.33

$\bullet\text{OH}/\text{O}_2^{\bullet-}$ in Eq. 1) by a factor of 2.3 and 24 in the “ KO_2 ” and “ $\text{KO}_2 + \text{Fe}$ ” treatments, respectively, and indicated an autocatalytic formation of $\bullet\text{OH}$ from $\text{O}_2^{\bullet-}$ in the presence of DOM-Fe.

4 Discussion

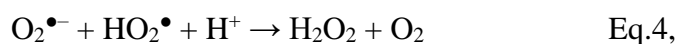
4.1 $\bullet\text{OH}$ production

As explained in the Method-section 2.2, the amount of introduced $\text{O}_2^{\bullet-}$ in this study is environmentally relevant but here we compare the cumulative productions of $\bullet\text{OH}$ (0.23–104 μM) in our week-long experiment to those reported earlier. An oxidation of reduced DOM or metals produces $\bullet\text{OH}$. For example, the oxidation of Arctic surface and soil waters produce 0.2–4.5 μM $\bullet\text{OH}$ over 24 hour oxidation (Page et al., 2013); the oxidation of hypolimnetic water accumulatively produces 0.2–4.5 μM $\bullet\text{OH}$ (Minella et al., 2015); the oxidation of pyrite can produce 7.5–135 μM $\bullet\text{OH}$ within 7 hours (Zhang & Yuan, 2017); and the oxidation of river sediments can accumulatively produce 57–1479 $\mu\text{mol kg}^{-1}$ $\bullet\text{OH}$ within 48 hours (Liao et al., 2019). Thus, the cumulative productions of $\bullet\text{OH}$ in this study are broadly similar to those reported earlier from various environmental processes.

4.2 Stoichiometric production of $\bullet\text{OH}$ from superoxide and DOM-Fe(III)

In this study, the production of $\bullet\text{OH}$ is orders of magnitude larger in the presence than the absence of introduced KO_2 , therefore, $\text{O}_2^{\bullet-}$ is responsible for the extensive production of $\bullet\text{OH}$. The reaction pathway from $\text{O}_2^{\bullet-}$ to $\bullet\text{OH}$ is beyond the scope of the present study, because we did not measure the intermediates such as DOM-Fe(II) or H_2O_2 . Our simple kinetic model, however, successfully predicts the measured $R_f^{\bullet\text{OH}}(t_0)$ in the “ $\text{KO}_2 + \text{Fe}$ ” treatment and may provide a mechanistic explanation for the initial $\bullet\text{OH}$ production rates (Text SI). According to this simple model, the reaction pathway starts with the reduction of DOM-Fe(III) to DOM-

Fe(II) by $\text{O}_2^{\bullet-}$ (Eq.3, Text SI). Later, bimolecular disproportionation generates H_2O_2 (Eq.4). At this stage, the reduction of O_2 by DOM-Fe(II) is the source of $\text{O}_2^{\bullet-}$ (Text SI). Finally, H_2O_2 reacts with DOM-Fe(II) (Eq.1, Text SI). The reactive oxygen species can maintain the redox cycling of the iron catalyst and the production of $\bullet\text{OH}$ from the oxidant ($\text{H}_2\text{O}_2 = 2[\text{O}_2^{\bullet-} + \text{H}^+]$) according to the stoichiometry of the Fenton reaction (Pignatello et al. 2006; Text SI).

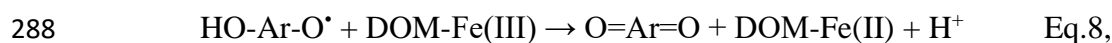
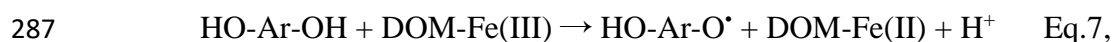
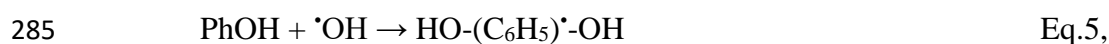


DOM facilitates the formation of $\bullet\text{OH}$ through the Fenton reaction in many ways (Georgi et al., 2007). When DOM makes complexes with Fe(III) at $\text{pH} > 3.5$, it keeps Fe(III) in soluble reactive form (Zhang & Zhou, 2019). At low pH (e.g., $\text{pH} = 5$ in this study), the deprotonated carboxylic groups of DOM are favorable ligand for Fe(III) and the concentration of a major competing ligand, hydroxyl ion (OH^-), is low (Bhattacharyya et al., 2019; Lee et al., 2019; Neubauer et al., 2013; Zhang & Zhou, 2019). Mildly acidic conditions (like in the present study) are favorable for the Fenton reaction, which breaks down humic substances most efficiently at $\text{pH} 4\text{--}5$ rather than in more acidic or basic solutions (Wu et al., 2010). Additionally, H_2O_2 reacts faster with DOM-Fe(II) than with inorganic Fe(II) (Voelker & Sulzberger 1996; Zhang & Zhou, 2019).

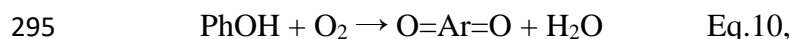
4.3 Autocatalysis of the Fenton reaction

In our study, the cumulative production of $\bullet\text{OH}$ is larger ($0.76\text{--}8 \bullet\text{OH}/\text{O}_2^{\bullet-}$) than expected from the introduced $\text{O}_2^{\bullet-}$ according to the stoichiometry of the Fenton reaction ($0.33 \bullet\text{OH}/\text{O}_2^{\bullet-}$). The reactions between $\bullet\text{OH}$ and the phenolic moieties of DOM can explain the autocatalysis of the Fenton reaction in this study (Voelker & Sulzberger, 1996, Chen & Pignatello, 1997). Those reactions generate hydroquinone-like DOM and $\text{O}_2^{\bullet-}$ (Voelker & Sulzberger, 1996, Chen & Pignatello, 1997, Duysterberg & Waite, 2007). The reactions

between $\bullet\text{OH}$ and phenols have been examined earlier with model compounds (phenol and hydroxybenzoic acid) that mimic the aromatic moieties of DOM (Chen & Pignatello, 1997; Duesterberg & Waite, 2007). Firstly, an addition of $\bullet\text{OH}$ to phenol (PhOH) generates a dihydroxycyclohexadienyl radical ($\text{HO}-(\text{C}_6\text{H}_5)\bullet\text{-OH}$, Eq.5), which transforms into hydroquinone (HO-Ar-OH) in a reaction that consumes O_2 and generates $\text{O}_2^{\bullet-}$ (Eq.6, Chen & Pignatello, 1997; Voelker & Sulzberger, 1996). Secondly, the transformation of hydroquinone to semiquinone radical ($\text{HO-Ar-O}\bullet$) reduces DOM-Fe(III) to DOM-Fe(II) (Eq.7, Chen & Pignatello, 1997; Duesterberg & Waite, 2007). Finally, a semiquinone radical reduces another DOM-Fe(III) when undergoing oxidation to quinone (O=Ar=O) (Eq.8, Chen & Pignatello, 1997; Duesterberg & Waite, 2007).



The four consecutive reactions (Eq.5-8) described above produce three reducing equivalents ($\text{O}_2^{\bullet-}$ and/or DOM-Fe(II)) that re-generate the Fenton reactants and thus the production of $\bullet\text{OH}$ gets autocatalyzed through the Fenton reaction and DOM oxidation. Note that the net reaction of this process (from Eq.1 to Eq.9, with the exception of Eq.2) is the oxidation of phenol to quinone (Eq.10).



This autocatalysis can continue as long as water contains O_2 and DOM contains aromatic moieties that $\bullet\text{OH}$ can transform into hydroquinones. In this study, the headspace of air serves as a source of dissolved O_2 to our solutions like the atmosphere is a source of O_2 to

surface waters. The high (45–67%) aromaticity of DOM used in this study (Vogt et al., 2004) provides a large reservoir of aromatic moieties that $\bullet\text{OH}$ can transform into hydroquinones. Because highly aromatic humic substances and Fe are abundant in soils and freshwaters, the potential for the autocatalyzed Fenton reaction is high in these environments.

4.4 Fenton reaction without introduced $\text{O}_2^{\bullet-}$

Our experiments show that even without introduction of $\text{O}_2^{\bullet-}$, DOM-Fe can produce hydroxyl radicals at low amounts that are similar to $< 0.5 \mu\text{M}$ $\bullet\text{OH}$ produced during aeration of Arctic surface waters (Page et al., 2012; Trusiak et al., 2018). Since Lake Valkea-Kotinen has typically anoxic hypolimnion in late summer and it is surrounded by peaty soils, the DOM extract used in the present study may contain Fe or quinone-like moieties in a reduced state. The reduced hydroquinone-like moieties or reduced metals (e.g., Fe(II)) associated to DOM can reduce O_2 to $\text{O}_2^{\bullet-}$ and initiate the sequence of reactions leading to the Fenton reaction (Garg et al., 2018; Page et al., 2013, 2014). In this study, the external supply of DOM-Fe(III) doubled the $\bullet\text{OH}$ production compared to DOM extract alone with low content of Fe and further emphasizes the Fenton reaction as a source of $\bullet\text{OH}$. Although an abiotic dark formation of $\bullet\text{OH}$ is low in oxic surface waters without external source of $\text{O}_2^{\bullet-}$ (Trusiak et al., 2018; this study), an episodic mixing of reduced DOM or redox sensitive metals to an oxic environment can promote an extensive production of $\bullet\text{OH}$ (Minella et al., 2015; Page et al., 2012, 2013; Trusiak et al., 2018).

4.5 Effects of $\text{O}_2^{\bullet-}$ and Fe on the absorption spectra of CDOM

In this study, the introduction of external $\text{O}_2^{\bullet-}$ eventually led to a CDOM break down and increased the value of $S_{275-295}$ (Figure 1). These changes in CDOM are related to the produced amount of $\bullet\text{OH}$ radicals and indicate that $\bullet\text{OH}$ rather than $\text{O}_2^{\bullet-}$ breaks down DOM (Goldstone et al., 2002; Pignatello et al., 2006; Rush & Bielski, 2005; Waggoner et al., 2017;

Wu et al., 2010; this study). The changes in CDOM found in this study indicate a breakdown of DOM into smaller less aromatic molecules (Helms et al., 2008) as found earlier in the reactions between DOM and $\bullet\text{OH}$ (Goldstone et al., 2002; Pignatello et al., 2006).

4.6 Effects of $\text{O}_2^{\bullet-}$ and Fe on the fluorescence spectra of CDOM

In our study, the introduction of KO_2 without external supply of Fe(III) increases the fluorescence of humic-like components (Figure 3), which agrees with the involvement of hydroquinones in the autocatalysis of the Fenton reaction (Chen & Pignatello, 1997; Duesterberg & Waite, 2007). The hydroxylation of aromatic moieties into hydroquinones by $\bullet\text{OH}$ can explain the increase in fluorescence and no change in absorption in the first 26 h (Figure 1a and 3), because hydroquinone-moieties have high fluorescence and absorption (Cory et al., 2005). Additionally, the breakdown of DOM by $\bullet\text{OH}$ decreases the molecular size of DOM and increases the spectral slope coefficient (Figure 1b), which are both related to an increase in the quantum yield of fluorescence (Boyle et al., 2009; Senesi, 1990). The complexation of Fe quenches fluorescence of DOM (Cabaniss, 1992; Du et al., 2018; Poulin et al., 2014; Pullin et al., 2007; Figure 3), because Fe promotes internal conversion and intersystem crossing of the first excited singlet state as well as a ligand to metal charge transfer, i.e., processes that compete with fluorescence (Senesi, 1990). The reduction in fluorescence in the “Fe + KO_2 ” treatment (Figure 3) is, instead, attributed to the breakdown of DOM by the extensive amount of $\bullet\text{OH}$, suggesting that there is an optimum in fluorescence emission as a function of DOM molecular weight or aromaticity.

5 Conclusions

This study shows that $\text{O}_2^{\bullet-}$ can induce the production of $\bullet\text{OH}$ in the presence of complexes between Fe and humic DOM. The production of $\bullet\text{OH}$ can exceed the stoichiometry of Fenton reaction by 2–24 folds. The autocatalysis of Fenton reaction observed in the present study

emphasizes the role of $O_2^{\bullet-}$ as an efficient transformer of organic matter. As numerous processes (photochemistry, abiotic dark oxidation, and biology) can produce $O_2^{\bullet-}$, superoxide-driven Fenton reactions likely transform natural organic matter and contaminants in diverse terrestrial and freshwater environments.

Author Contributions

Y.X., L.C., and A.V.V. all contributed to the preparation, writing, and editing the manuscript. Y.X. and M.-T.N. contributed to the sample collection and measurements. All authors reviewed the manuscript.

Declaration of competing interest

The authors declare no competing financial interest.

Acknowledgements

This study was financially supported by the Academy of Finland Grant (No. 295709) and Taishan Scholar Foundation of Shandong Province (No. tsqn201909126). The stay of L.C. in Jyväskylä was financially supported by the Erasmus+ Traineeship programme. L.C. acknowledges Compagnia di San Paolo (Torino, Italy) for financially supporting his Ph.D. fellowship.

Appendix A. Supplementary data

Supplementary data to this article can be found online at ***.

References

Aarnos, H., Gélinas, Y., Kasurinen, V., Gu, Y., Puupponen, V.-M., & Vähätalo, A. V. (2018).

373 Photochemical Mineralization of Terrigenous DOC to Dissolved Inorganic Carbon in
 374 Ocean. *Global Biogeochemical Cycles*, 32(2), 250–266.
 375 <https://doi.org/10.1002/2017GB005698>

376 Aeschbacher, M., Schwarzenbach, R. P., & Sander, M. (2010). Novel electrochemical
 377 approach to quantify the redox state of humic substances: Advantages and applications.
 378 *Environmental Science & Technology*, 44(1), 87–93.

379 Arnosti, C. (2004). Speed bumps and barricades in the carbon cycle: Substrate structural
 380 effects on carbon cycling. *Marine Chemistry*, 92(1-4 SPEC. ISS.), 263–273.
 381 <https://doi.org/10.1016/j.marchem.2004.06.030>

382 Bhattacharyya, A., Schmidt, M. P., Stavitski, E., Azimzadeh, B., & Martínez, C. E. (2019).
 383 Ligands representing important functional groups of natural organic matter facilitate Fe
 384 redox transformations and resulting binding environments. *Geochimica et*
 385 *Cosmochimica Acta*, 251, 157–175. <https://doi.org/10.1016/J.GCA.2019.02.027>

386 Boyle, E. S., Guerriero, N., Thiallet, A., Vecchio, R. Del, & Blough, N. V. (2009). Optical
 387 Properties of Humic Substances and CDOM: Relation to Structure. *Environmental*
 388 *Science & Technology*, 43(7), 2262–2268. <https://doi.org/10.1021/es803264g>

389 Burgos Castillo, R. C., Fontmorin, J. M., Tang Walter, Z., Xochitl, D. B., & Mika, S. (2018).
 390 Towards reliable quantification of hydroxyl radicals in the Fenton reaction using
 391 chemical probes. *RSC Advances*, 8(10), 5321–5330. <https://doi.org/10.1039/c7ra13209c>

392 Cabaniss, S. E. (1992). Synchronous fluorescence-spectra of metal-fulvic acid complexes.
 393 *Environ. Sci. Technol.*, 26(6), 1133–1139.

394 Chen, R., & Pignatello, J. J. (1997). Role of quinone intermediates as electron shuttles in
 395 Fenton and photoassisted Fenton oxidations of aromatic compounds. *Environmental*
 396 *Science & Technology*, 31, 2399–2406. <https://doi.org/10.1021/ES9610646>

397 Cooper, W. J., & Zika, R. G. (1983). Photochemical formation of hydrogen peroxide in

- surface and ground waters exposed to sunlight. *Science*, 220(4598), 711–712.
<https://doi.org/10.1126/science.220.4598.711>
- Cory, R. M., McKnight, D. M., And, R. M. C., & McKnight, D. M. (2005). Fluorescence spectroscopy reveals ubiquitous presence of oxidized and reduced quinones in dissolved organic matter. *Environmental Science & Technology*, 39(21), 8142–8149.
<https://doi.org/10.1021/ES0506962>
- Diaz, J. M., Hansel, C. M., Voelker, B. M., Mendes, C. M., Andeer, P. F., & Zhang, T. (2013). Widespread production of extracellular superoxide by heterotrophic bacteria. *Science*, 340(6137), 1223–1226. <https://doi.org/10.1126/science.1237331>
- Diaz, Julia M., & Plummer, S. (2018). Production of extracellular reactive oxygen species by phytoplankton: past and future directions. *Journal of Plankton Research*, 40, 655–666.
<https://doi.org/10.1093/plankt/fby039>
- Dittmar, T., Koch, B., Hertkorn, N., & Kattner, G. (2008). A simple and efficient method for the solid-phase extraction of dissolved organic matter (SPE-DOM) from seawater. *Limnology and Oceanography: Methods*, 6(6), 230–235.
<https://doi.org/10.4319/lom.2008.6.230>
- Du, Y., Ramirez, C. E., & Jaffé, R. (2018). Fractionation of dissolved organic matter by co-precipitation with iron: Effects of composition. *Environmental Processes*, 5(1), 5–21.
<https://doi.org/10.1007/s40710-017-0281-4>
- Duesterberg, C. K., & Waite, T. D. (2007). Kinetic modeling of the oxidation of p - hydroxybenzoic acid by Fenton’s reagent: Implications of the role of quinones in the Redox cycling of iron. *Environmental Science & Technology*, 41(11), 4103–4110.
<https://doi.org/10.1021/es0628699>
- Einola, E., Rantakari, M., Kankaala, P., Kortelainen, P., Ojala, A., Pajunen, H., et al. (2011). Carbon pools and fluxes in a chain of five boreal lakes: A dry and wet year comparison.

Journal of Geophysical Research: Biogeosciences, 116(3).

<https://doi.org/10.1029/2010JG001636>

Fujii, M., & Otani, E. (2017). Photochemical generation and decay kinetics of superoxide and hydrogen peroxide in the presence of standard humic and fulvic acids. *Water Research*, 123, 642–654. <https://doi.org/10.1016/j.watres.2017.07.015>

Fujii, M., Imaoka, A., Yoshimura, C., & Waite, T. D. (2014). Effects of molecular composition of natural organic matter on ferric iron complexation at circumneutral pH. *Environmental Science and Technology*, 48(8), 4414–4424. <https://doi.org/10.1021/es405496b>

Gao, H., & Zepp, R. G. (1998). Factors influencing photoreactions of dissolved organic matter in a coastal river of the southeastern United States. *Environmental Science & Technology*, 32, 2940–2946. Retrieved from <https://pubs.acs.org/sharingguidelines>

Garg, S., Rose, A. L., & Waite, T. D. (2011). Photochemical production of superoxide and hydrogen peroxide from natural organic matter. *Geochimica et Cosmochimica Acta*, 75(15), 4310–4320. <https://doi.org/10.1016/j.gca.2011.05.014>

Garg, S., Jiang, C., & Waite, T. D. (2018). Impact of pH on iron redox transformations in simulated freshwaters containing natural organic matter. *Environmental Science and Technology*, 52(22), 13184–13194. research-article. <https://doi.org/10.1021/acs.est.8b03855>

Georgi, A., Schierz, A., Trommler, U., Horwitz, C. P., Collins, T. J., & Kopinke, F. D. (2007). Humic acid modified Fenton reagent for enhancement of the working pH range. *Applied Catalysis B: Environmental*, 72(1–2), 26–36. <https://doi.org/10.1016/j.apcatb.2006.10.009>

Gil-Lozano, C., Davila, A. F., Losa-Adams, E., Fairén, A. G., & Gago-Duport, L. (2017). Quantifying Fenton reaction pathways driven by self-generated H₂ O₂ on pyrite

surfaces. *Scientific Reports*, 7. <https://doi.org/10.1038/srep43703>

Goldstone, J. V., Pullin, M. J., Bertilsson, S., Voelker, B. M., & Hole, W. (2002). Reactions of hydroxyl radical with humic substances : Bleaching , mineralization , and production of bioavailable carbon substrates, *36*(3), 364–372. <https://doi.org/10.1021/ES0109646>

Goldstone, Jared V., & Voelker, B. M. (2000). Chemistry of superoxide radical in seawater: CDOM associated sink of superoxide in coastal waters. *Environmental Science and Technology*, *34*(6), 1043–1048. <https://doi.org/10.1021/es9905445>

Hayyan, M., Hashim, M. A., & AlNashef, I. M. (2016). Superoxide Ion: Generation and Chemical Implications. *Chemical Reviews*, *116*(5), 3029–3085. <https://doi.org/10.1021/acs.chemrev.5b00407>

Helms, J. R., Stubbins, A., Ritchie, J. D., Minor, E. C., Kieber, D. J., & Mopper, K. (2008). Absorption spectral slopes and slope ratios as indicators of molecular weight, source, and photobleaching of chromophoric dissolved organic matter. *Limnology and Oceanography*, *53*(3), 955–969. <https://doi.org/10.4319/lo.2008.53.3.0955>

Hongve, D., Riise, G., & Kristiansen, J. F. (2004). Increased colour and organic acid concentrations in Norwegian forest lakes and drinking water - A result of increased precipitation? *Aquatic Sciences*, *66*(2), 231–238. <https://doi.org/10.1007/s00027-004-0708-7>

Imlay, J. A. (2004). Pathways of Oxidative Damage. *Annual Review of Microbiology*, *57*(1), 395–418. <https://doi.org/10.1146/annurev.micro.57.030502.090938>

Karlsson, T., & Persson, P. (2012). Complexes with aquatic organic matter suppress hydrolysis and precipitation of Fe(III). *Chemical Geology*, *322–323*, 19–27. <https://doi.org/10.1016/j.chemgeo.2012.06.003>

Koehler, B., Landelius, T., Weyhenmeyer, G. A., Machida, N., & Tranvik, L. J. (2014). Sunlight-induced carbon dioxide emissions from inland waters. *Global Biogeochemical*

473 *Cycles*, 28(7), 696–711. <https://doi.org/10.1002/2014GB004850>

474 Kothawala, D., Kellerman, A., Catalan, N., & Tranvik, L. (2016). Controls on the dynamics
475 of dissolved organic matter in boreal lakes. *Geophysical Research Abstracts EGU*
476 *General Assembly*, 18(April), 13894. [https://doi.org/10.1097/00010694-200004000-](https://doi.org/10.1097/00010694-200004000-00001)
477 00001

478 Lee, S., Roh, Y., & Koh, D.-C. (2019). Oxidation and reduction of redox-sensitive elements
479 in the presence of humic substances in subsurface environments: A review.
480 *Chemosphere*, 220, 86–97. <https://doi.org/10.1016/j.chemosphere.2018.11.143>

481 Liao, P., Yu, K., Lu, Y., Wang, P., Liang, Y., & Shi, Z. (2019). Extensive dark production of
482 hydroxyl radicals from oxygenation of polluted river sediments. *Chemical Engineering*
483 *Journal*, 368, 700–709. <https://doi.org/10.1016/j.cej.2019.03.018>

484 Louit, G., Foley, S., Cabillic, J., Coffigny, H., Taran, F., Valleix, A., et al. (2005). The
485 reaction of coumarin with the OH radical revisited: Hydroxylation product analysis
486 determined by fluorescence and chromatography. *Radiation Physics and Chemistry*,
487 72(2–3), 119–124. <https://doi.org/10.1016/j.radphyschem.2004.09.007>

488 Ma, J., Del Vecchio, R., Golanoski, K. S., Boyle, E. S., & Blough, N. V. (2010). Optical
489 properties of humic substances and CDOM: Effects of borohydride reduction.
490 *Environmental Science & Technology*, 44(14), 5395–5402.
491 <https://doi.org/10.1021/es100880q>

492 Micinski, E., Ball, L. A., & Zafiriou, O. C. (1993). Photochemical oxygen activation:
493 Superoxide radical detection and production rates in the eastern Caribbean. *Journal of*
494 *Geophysical Research: Oceans*, 98(C2), 2299–2306.
495 [https://doi.org/10.1029/92JC02766@10.1002/\(ISSN\)2169-9291.PECW1](https://doi.org/10.1029/92JC02766@10.1002/(ISSN)2169-9291.PECW1)

496 Minella, M., De Laurentiis, E., Maurino, V., Minero, C., & Vione, D. (2015). Dark
497 production of hydroxyl radicals by aeration of anoxic lake water. *Science of the Total*

498 *Environment*, 527–528, 322–327. <https://doi.org/10.1016/j.scitotenv.2015.04.123>

499 Mostovaya, A., Hawkes, J. A., Dittmar, T., & Tranvik, L. J. (2017). Molecular determinants
500 of dissolved organic matter reactivity in lake water. *Frontiers in Earth Science*, 5.
501 <https://doi.org/10.3389/feart.2017.00106>

502 Murphy, K. R., Stedmon, C. A., Graeber, D., & Bro, R. (2013). Fluorescence spectroscopy
503 and multi-way techniques. PARAFAC. *Analytical Methods*, 5(23), 6557.
504 <https://doi.org/10.1039/c3ay41160e>

505 Neubauer, E., Köhler, S. J., von der Kammer, F., Laudon, H., Hofmann, T., Neubauer, E., et
506 al. (2013). Effect of pH and stream order on iron and arsenic speciation in boreal
507 catchments. *Environmental Science & Technology*, 47(13), 1–14.
508 <https://doi.org/10.1021/es401193j>

509 Page, S. E., Sander, M., Arnold, W. A., & McNeill, K. (2012). Hydroxyl radical formation
510 upon oxidation of reduced humic acids by oxygen in the dark. *Environmental Science
511 and Technology*, 46(3), 1590–1597. <https://doi.org/10.1021/es203836f>

512 Page, S. E., Kling, G. W., Sander, M., Harrold, K. H., Logan, J. R., McNeill, K., & Cory, R.
513 M. (2013). Dark formation of hydroxyl radical in arctic soil and surface waters.
514 *Environmental Science and Technology*, 47(22), 12860–12867.
515 <https://doi.org/10.1021/es4033265>

516 Page, S. E., Logan, J. R., Cory, R. M., & McNeill, K. (2014). Evidence for dissolved organic
517 matter as the primary source and sink of photochemically produced hydroxyl radical in
518 arctic surface waters. *Environmental Sciences: Processes and Impacts*, 16(4), 807–822.
519 <https://doi.org/10.1039/c3em00596h>

520 Piccolo, A. (1996). *Humic substances in terrestrial ecosystems*. Amsterdam.

521 Pignatello, J. J., Oliveros, E., & MacKay, A. (2006). Advanced oxidation processes for
522 organic contaminant destruction based on the fenton reaction and related chemistry.

523 *Critical Reviews in Environmental Science and Technology*, 36(1), 1–84.
 524 <https://doi.org/10.1080/10643380500326564>

525 Poulin, B. A., Ryan, J. N., & Aiken, G. R. (2014). The effects of iron on optical properties of
 526 dissolved organic matter. *Environmental Science & Technology*, 48(17), 10098–10106.
 527 <https://doi.org/10.1021/es502670r>

528 Pullin, M. J., Anthony, C., & Maurice, P. A. (2007). Effects of iron on the molecular weight
 529 distribution, light absorption, and fluorescence properties of natural organic matter.
 530 *Environmental Engineering Science*, 24(8), 987–997.
 531 <https://doi.org/10.1089/ees.2006.0040>

532 Rose, A. L., & Waite, T. D. (2005). Reduction of organically complexed ferric iron by
 533 superoxide in a simulated natural water. *Environmental Science & Technology*,
 534 39(February), 2645–2650. <https://doi.org/10.1021/es048765k>

535 Rush, J. D., & Bielski, B. H. J. (2005). Pulse radiolytic studies of the reaction of
 536 perhydroxyl/superoxide O₂⁻ with iron(II)/iron(III) ions. The reactivity of HO₂/O₂⁻ with
 537 ferric ions and its implication on the occurrence of the Haber-Weiss reaction. *The*
 538 *Journal of Physical Chemistry*, 89(23), 5062–5066. <https://doi.org/10.1021/j100269a035>

539 Senesi, N. (1990). Molecular and quantitative aspects of the chemistry of fulvic acid and its
 540 interactions with metal ions and organic chemicals. *Analytica Chimica Acta*, 232, 77–
 541 106. [https://doi.org/10.1016/S0003-2670\(00\)81226-X](https://doi.org/10.1016/S0003-2670(00)81226-X)

542 Southworth, B. A., & Voelker, B. M. (2003). Hydroxyl radical production via the photo-
 543 Fenton reaction in the presence of fulvic acid. *Environmental Science & Technology*,
 544 37(6), 1130–1136. <https://doi.org/10.1021/es020757l>

545 Tranvik, L. J. (1988). Availability of dissolved organic carbon for planktonic bacteria in
 546 oligotrophic lakes of differing humic content. *Microbial Ecology*, 16(3), 311–322.
 547 <https://doi.org/10.1007/BF02011702>

548 Trusiak, A., Treibergs, L. A., Kling, G. W., & Cory, R. M. (2018). The role of iron and
 549 reactive oxygen species in the production of CO₂ in arctic soil waters. *Geochimica et*
 550 *Cosmochimica Acta*, 224, 80–95. <https://doi.org/10.1016/j.gca.2017.12.022>
 551 Vähätalo, A. V., Salonen, K., Münster, U., Järvinen, M., & Wetzel, R. G. (2003).
 552 Photochemical transformation of allochthonous organic matter provides bioavailable
 553 nutrients in a humic lake. *Archiv Fur Hydrobiologie*, 156(3), 287–314.
 554 <https://doi.org/10.1127/0003-9136/2003/0156-0287>
 555 Voelker, B. M., & Sulzberger, B. (1996). Effects of fulvic acid on Fe(II) oxidation by
 556 hydrogen peroxide. *Environmental Science and Technology*, 30(4), 1106–1114.
 557 <https://doi.org/10.1021/es9502132>
 558 Voelker, B. M., Morel, F. M. M., & Sulzberger, B. (1997). Iron redox cycling in surface
 559 waters: Effects of humic substances and light. *Environmental Science and Technology*,
 560 31(4), 1004–1011. <https://doi.org/10.1021/es9604018>
 561 Vogt, R. D., Akkanen, J., Andersen, D. O., Brüggemann, R., Chatterjee, B., Gjessing, E., et
 562 al. (2004). Key site variables governing the functional characteristics of Dissolved
 563 Natural Organic Matter (DNOM) in Nordic forested catchments. *Aquatic Sciences -*
 564 *Research Across Boundaries*, 66(2), 195–210. [https://doi.org/10.1007/s00027-004-0710-](https://doi.org/10.1007/s00027-004-0710-0)
 565 0
 566 Waggoner, D. C., Wozniak, A. S., Cory, R. M., & Hatcher, P. G. (2017). The role of reactive
 567 oxygen species in the degradation of lignin derived dissolved organic matter.
 568 *Geochimica et Cosmochimica Acta*, 208, 171–184.
 569 <https://doi.org/10.1016/j.gca.2017.03.036>
 570 Wu, Y., Zhou, S., Qin, F., Peng, H., Lai, Y., & Lin, Y. (2010). Removal of humic substances
 571 from landfill leachate by Fenton oxidation and coagulation. *Process Safety and*
 572 *Environmental Protection*, 88(4), 276–284. <https://doi.org/10.1016/j.psep.2010.03.002>

- Yuan, X., Davis, J. A., & Nico, P. S. (2016). Iron-mediated oxidation of Methoxyhydroquinone under dark conditions: Kinetic and mechanistic insights. *Environmental Science and Technology*, 50(4), 1731–1740. <https://doi.org/10.1021/acs.est.5b03939>
- Zhang, P., & Yuan, S. (2017). Production of hydroxyl radicals from abiotic oxidation of pyrite by oxygen under circumneutral conditions in the presence of low-molecular-weight organic acids. *Geochimica et Cosmochimica Acta*, 218, 153–166. <https://doi.org/10.1016/j.gca.2017.08.032>
- Zhang, T., Hansel, C. M., Voelker, B. M., & Lamborg, C. H. (2016). Extensive dark biological production of reactive oxygen species in brackish and freshwater ponds. *Environmental Science and Technology*, 50(6), 2983–2993. <https://doi.org/10.1021/acs.est.5b03906>
- Zhang, Yi, & Blough, N. V. (2016). Photoproduction of one-electron reducing intermediates by chromophoric dissolved organic matter (CDOM): Relation to O₂- and H₂O₂ photoproduction and CDOM photooxidation. *Environmental Science and Technology*, 50(20), 11008–11015. <https://doi.org/10.1021/acs.est.6b02919>
- Zhang, Ying, & Zhou, M. (2019). A critical review of the application of chelating agents to enable Fenton and Fenton-like reactions at high pH values. *Journal of Hazardous Materials*, 362, 436–450. <https://doi.org/10.1016/j.jhazmat.2018.09.035>

Tables

Table 1. Experimental design. The initial concentrations of DOM, complexed Fe, KO₂, and coumarin in the treatments made in artificial lake water (Table S1).

| Treatments | DOM (mg L ⁻¹) | Fe (μM) | KO ₂ (μM) | Coumarin (μM) |
|------------------------------------|------------------------------|-------------------|-------------------------|------------------|
| control | 20 | 0.17 [*] | -- | 10 |
| KO ₂ ^{***} | 20 | 0.17 [*] | 13 | 10 |
| Fe | 20 | 20 ^{**} | -- | 10 |
| Fe + KO ₂ ^{**} | 20 | 20 ^{**} | 13 | 10 |

--, no addition of KO₂. ^{*} residual Fe in extracted DOM (8.5 nmol Fe/mg DOM), ^{**} introduced as DOM-Fe complex. ^{***} In the treatments “KO₂” and “Fe + KO₂”, the introduction of 13 μM KO₂ increased pH to 12.2, which was soon titrated with HCl back to the same pH 5 as in the other treatments.

601 **Table 2.** Cumulative production of •OH radicals (μM) in the treatments.
602

| Time Interval | control | Fe | KO ₂ | Fe + KO ₂ |
|------------------|---------|------|-----------------|----------------------|
| 0–10 h | 0.09 | 0.11 | 1.32 | 16.3 |
| 0–168 h | 0.23 | 0.57 | 9.88 | 103.5 |

603

Figure captions

Figure 1. Absorption coefficient of CDOM at 410 nm (a_{410}) and spectral slope coefficient ($S_{275-295}$) after 26 h and 168 h incubations in the three treatments and the control. Table 1 explains the treatments. Stars indicate a significant difference between the treatments and the control, * $P < 0.05$ and ** $P < 0.01$. Error bars show standard deviations of three replicated treatments.

Figure 2. Overlaid spectra of four components (PARAFAC model). The figure shows six unique splits vs. the overall model. Dot lines indicate excitation spectra and solid lines indicate emission spectra. The excitation and emission maxima of each components are shown in Table S2. The loadings in the Y-axis indicate the normalized component intensity in the PARAFAC modeling.

Figure 3. Fluorescent intensities at 168 h of four components obtained from EEM-PARAFAC modeling (Figure 2). The fluorescence of component 4 was negligible in the “Fe+KO₂” treatment. Stars indicate a significant difference between treatment and the control, * $P < 0.05$ and ** $P < 0.01$. Error bars show standard deviations of three replicated treatments.

Figure 4. Computed formation rate of •OH in the treatments at selected times (■). The blue lines represent the fitting functions from which the cumulative production of •OH radicals were calculated. The R^2 parameter shows the goodness of the fit. See SI for the fitting functions. Note the orders of magnitude differences in the scales of Y-axes.